

SM fermions	Vector-like leptons	Scalars
$q_L = (u \ d)_L \sim (1/6, Y'_q)$	$(N_1 \ E_1)_L \sim (-1/2, -9Y'_q/2)$	$\Phi_1 \sim (1/2, 9Y'_q)$
$u_R \sim (2/3, Y'_q)$	$(N_1 \ E_1)_R \sim (-1/2, 9Y'_q/2)$	$\Phi_2 \sim (1/2, 0)$
$d_R \sim (-1/3, Y'_q)$	$N_{2L} \sim (0, 9Y'_q/2)$	$\chi \sim (0, 9Y'_q)$
$\ell_L = (\nu_l \ l)_L \sim (-1/2, 0)$	$N_{2R} \sim (0, -9Y'_q/2)$	
$l_R \sim (-1, 0)$	$E_{2L} \sim (-1, 9Y'_q/2)$	
	$E_{2R} \sim (-1, -9Y'_q/2)$	

TABLE I. SM and U(1)' hypercharges $\psi \sim (Y, Y')$ of the fermions and scalars in the UN2HDM. Generation indices in SM fermions are omitted, as well as colour indices for quarks.

cade decays like the one in Eq. (1) cannot take place if both doublets have vanishing U(1)' hypercharge. On the other hand, due to the requirements of U(1)' gauge invariance of the Yukawa terms of SM leptons, and of a leptophobic Z' , one of the Higgs doublets must have zero hypercharge under U(1)'. We therefore label the scalar doublets so that $Y'_{\Phi_2} = 0$ and $Y'_{\Phi_1} \neq 0$. The U(1)' gauge invariance of the quark Yukawa terms with Φ_2 implies $Y'_q = Y'_u = Y'_d$, generally non-vanishing. Therefore, we have the same Yukawa lagrangian found in a Type I two-Higgs doublet model (2HDM), namely

$$-\mathcal{L}_Y = Y_u \bar{q}_L \tilde{\Phi}_2 u_R + Y_d \bar{q}_L \Phi_2 d_R + Y_e \bar{\ell}_L \Phi_2 e_R + \text{h.c.} \quad (2)$$

The U(1)' hypercharges of SM fermions are identical to those of MSBMs. Thus, all U(1)' anomalies [21] cancel by adding the same extra matter as in MSBMs. Assuming the extra matter to be vector-like under the SM group, two simple solutions have been proposed in ref. [11]: one with a set of vector-like quarks (Model 1), and another with a set of vector-like leptons (Model 2). In this work we will concentrate only on Model 2, for which the field content and hypercharge assignments are given in Table I. The new vector-like leptons are the two SU(2) doublets $(N_1 \ E_1)_{L,R}$ and the four singlets $N_{2L,R}$ and $E_{2L,R}$. N_i and E_i have electric charge 0 and -1, respectively. Their hypercharges are fixed by anomaly cancellation, and all take values of $\pm 9Y'_q/2$. Gauge invariance of the Yukawa interactions of the new leptons with the scalar singlet (which give rise to their masses) implies

$$Y'_\chi = 9Y'_q. \quad (3)$$

We also assume a 'dark lepton number' that forbids Majorana mass terms for N_{2L} and N_{2R} [22]. Finally, as we will see later, a valid scalar mass spectrum can only be obtained if $Y'_{\Phi_1} = Y'_\chi$.

With these U(1)' hypercharge assignments, the most general gauge-invariant scalar potential of the UN2HDM is

$$V = m_{11}^2 \Phi_1^\dagger \Phi_1 + m_{22}^2 \Phi_2^\dagger \Phi_2 + \frac{m_0^2}{2} \chi^\dagger \chi + \frac{\lambda_1}{2} (\Phi_1^\dagger \Phi_1)^2 + \frac{\lambda_2}{2} (\Phi_2^\dagger \Phi_2)^2 + \lambda_3 (\Phi_1^\dagger \Phi_1) (\Phi_2^\dagger \Phi_2)$$

$$+ \lambda_4 (\Phi_1^\dagger \Phi_2) (\Phi_2^\dagger \Phi_1) + \frac{\lambda_5}{2} (\chi^\dagger \chi)^2 + \frac{\lambda_6}{2} (\Phi_1^\dagger \Phi_1) (\chi^\dagger \chi) + \frac{\lambda_7}{2} (\Phi_2^\dagger \Phi_2) (\chi^\dagger \chi) + (\mu \chi \Phi_1^\dagger \Phi_2 + \text{h.c.}), \quad (4)$$

where μ can be a complex parameter, while the remaining parameters are real. We define the scalar doublets $\Phi_{1,2}$ and singlet χ as

$$\Phi_k = \frac{1}{\sqrt{2}} \begin{pmatrix} \sqrt{2} \phi_k^+ \\ v_k e^{i\varphi_k} + \rho_k + i\eta_k \end{pmatrix}, \quad (k=1,2), \quad (5)$$

$$\chi = \frac{1}{\sqrt{2}} (u e^{i\varphi_3} + \rho_3 + i\eta_3).$$

Without loss of generality, one can assume $\varphi_1 = 0$, such that the vacuum expectation values (VEVs) are

$$\langle \Phi_1 \rangle = \frac{1}{\sqrt{2}} \begin{pmatrix} 0 \\ v_1 \end{pmatrix}, \quad \langle \Phi_2 \rangle = \frac{1}{\sqrt{2}} \begin{pmatrix} 0 \\ v_2 e^{i\varphi_2} \end{pmatrix} \quad (6)$$

$$\langle \chi \rangle = \frac{1}{\sqrt{2}} u e^{i\varphi_3}.$$

Throughout this work, we will always assume nonzero VEVs v_1 , v_2 and u . Note also that φ_2 and φ_3 can be rephased away through

$$\Phi_2 \rightarrow \Phi'_2 = e^{-i\varphi_2} \Phi_2, \quad \chi \rightarrow \chi' = e^{-i\varphi_3} \chi, \quad (7)$$

which leaves V invariant, provided μ is replaced by

$$\mu \rightarrow \mu' = \mu e^{-i(\varphi_2 + \varphi_3)}, \quad (8)$$

when V is expressed in terms of Φ'_2 and χ' . Since μ is an arbitrary complex parameter, from now on we assume $\varphi_2 = \varphi_3 = 0$ without loss of generality, therefore having all VEVs real.

An useful feature of V is that the number of parameters is equal to the number of physical quantities (masses and mixing angles) needed to define the Higgs sector. This means that all eleven parameters shown in Eq. (4) can be written in terms of the three VEVs v_1 , v_2 and u , as well as of the five scalar masses and three mixing angles that will be introduced later on.

For the cases we are interested in with $v_1, v_2, u \neq 0$, the four minimisation conditions of the scalar potential

are

$$\begin{aligned}
m_{11}^2 + \frac{v_1^2}{2}\lambda_1 + \frac{v_2^2}{2}(\lambda_3 + \lambda_4) + \frac{u^2}{4}\lambda_6 + \frac{u}{\sqrt{2}}\frac{v_2}{v_1}\Re(\mu) &= 0, \\
m_{22}^2 + \frac{v_2^2}{2}\lambda_2 + \frac{v_1^2}{2}(\lambda_3 + \lambda_4) + \frac{u^2}{4}\lambda_7 + \frac{u}{\sqrt{2}}\frac{v_1}{v_2}\Re(\mu) &= 0, \\
m_0^2 + u^2\lambda_5 + \frac{1}{2}v_1^2\lambda_6 + \frac{1}{2}v_2^2\lambda_7 + \sqrt{2}\frac{v_1v_2}{u}\Re(\mu) &= 0, \\
\Im(\mu) &= 0.
\end{aligned} \tag{9}$$

The first three equations allow to write m_{11}^2 , m_{22}^2 and m_0^2 in terms of the VEVs and the remaining parameters of the potential. The last equation in (9) implies that all parameters in the potential are real and, thus, there are no mixed $\rho_i\eta_j$ mass terms. Then, the 6×6 neutral scalar mass matrix can be written in block-diagonal form as

$$\mathcal{M}^n = \begin{pmatrix} M^\rho & 0 \\ 0 & M^\eta \end{pmatrix}, \tag{10}$$

where M^ρ and M^η are 3×3 real symmetric matrices defined in the (ρ_1, ρ_2, ρ_3) and (η_1, η_2, η_3) bases, respectively. Using henceforth the definitions

$$v = \sqrt{v_1^2 + v_2^2}, \quad \tan \beta = v_2/v_1, \tag{11}$$

and the notation $s_\beta = \sin \beta$, $c_\beta = \cos \beta$, the independent elements of M^ρ read

$$\begin{aligned}
M_{11}^\rho &= v^2\lambda_1c_\beta^2 - \frac{1}{\sqrt{2}}u\mu \tan \beta, \\
M_{12}^\rho &= v^2(\lambda_3 + \lambda_4)s_\beta c_\beta + \frac{1}{\sqrt{2}}u\mu, \\
M_{13}^\rho &= \frac{v}{2}u\lambda_6c_\beta + \frac{1}{\sqrt{2}}v\mu s_\beta, \\
M_{22}^\rho &= v^2\lambda_2s_\beta^2 - \frac{u\mu}{\sqrt{2}\tan \beta}, \\
M_{23}^\rho &= \frac{v}{2}u\lambda_7s_\beta + \frac{1}{\sqrt{2}}v\mu c_\beta, \\
M_{33}^\rho &= \lambda_5u^2 - \frac{1}{\sqrt{2}}\frac{v^2}{u}\mu c_\beta s_\beta,
\end{aligned} \tag{12}$$

while for M^η ,

$$\begin{aligned}
M_{11}^\eta &= -\frac{1}{\sqrt{2}}u\mu\frac{s_\beta}{c_\beta} & M_{12}^\eta &= \frac{1}{\sqrt{2}}u\mu, \\
M_{13}^\eta &= \frac{1}{\sqrt{2}}v\mu s_\beta, & M_{22}^\eta &= -\frac{1}{\sqrt{2}}u\mu\frac{c_\beta}{s_\beta}, \\
M_{23}^\eta &= -\frac{1}{\sqrt{2}}v\mu c_\beta, & M_{33}^\eta &= -\frac{1}{\sqrt{2}}\frac{v^2}{u}\mu c_\beta s_\beta.
\end{aligned} \tag{13}$$

All terms in M^η are proportional to μ , which explains the need to set $Y'_{\Phi_1} = Y'_\chi$, otherwise the μ term in (4) would not be present and we would have a massless scalar.

The matrix M^η is diagonalised as $R^T M^\eta R = (M^\eta)_{\text{diag}}$, using a rotation

$$R = \begin{pmatrix} -s_\beta & c_\beta & 0 \\ c_\beta & s_\beta & 0 \\ 0 & 0 & 1 \end{pmatrix} \begin{pmatrix} -s_\alpha & 0 & c_\alpha \\ 0 & 1 & 0 \\ c_\alpha & 0 & s_\alpha \end{pmatrix}, \tag{14}$$

being α given by

$$\tan \alpha = -\frac{u}{vc_\beta s_\beta}. \tag{15}$$

The only non-zero eigenvalue is

$$m_{A^0}^2 = -\frac{\mu}{\sqrt{2}} \left[\frac{u}{s_\beta c_\beta} + \frac{s_\beta c_\beta v^2}{u} \right], \tag{16}$$

which corresponds to the squared mass of a CP-odd scalar A^0 . The matrix O that rotates the ρ_i fields to the mass basis is parameterised by three mixing angles, $\alpha_1, \alpha_2, \alpha_3$, and it is given by

$$O = \begin{pmatrix} c_1c_2 & s_1c_2 & s_2 \\ -c_1s_2s_3 - s_1c_3 & c_1c_3 - s_1s_2s_3 & c_2s_3 \\ -c_1s_2c_3 + s_1s_3 & -c_1s_3 - s_1s_2c_3 & c_2c_3 \end{pmatrix}^T, \tag{17}$$

where $c_{1,2,3} = \cos \alpha_{1,2,3}$, $s_{1,2,3} = \sin \alpha_{1,2,3}$ and $-\pi/2 \leq \alpha_{1,2,3} \leq \pi/2$. Let us label as h the SM-like Higgs boson and $H_{1,2}$ the new CP-even scalars, with H_1 and H_2 being always defined in such a way that $m_{H_1} < m_{H_2}$. We can write M^ρ in terms of the masses of those three scalars and the three mixing angles introduced in Eq. (17). Namely,

$$M^\rho = O \begin{pmatrix} m_h^2 & 0 & 0 \\ 0 & m_{H_1}^2 & 0 \\ 0 & 0 & m_{H_2}^2 \end{pmatrix} O^T. \tag{18}$$

Finally, the charged-scalar mass matrix in the basis (ϕ_1^\pm, ϕ_2^\pm) is

$$\mathcal{M}^c = \left[v^2\lambda_4 + \frac{\sqrt{2}u\mu}{s_\beta c_\beta} \right] \begin{pmatrix} -s_\beta^2 & s_\beta c_\beta \\ s_\beta c_\beta & -c_\beta^2 \end{pmatrix}, \tag{19}$$

and its diagonalisation is performed as $U^T \mathcal{M}^c U = (\mathcal{M}^c)_{\text{diag}}$, with

$$U = \begin{pmatrix} -s_\beta & c_\beta \\ c_\beta & s_\beta \end{pmatrix}, \tag{20}$$

like in 2HDMs. The non-zero eigenvalue of \mathcal{M}^c is

$$m_{H^\pm}^2 = -\lambda_4 v^2 - \frac{\sqrt{2}u\mu}{c_\beta s_\beta}, \tag{21}$$

corresponding to the squared mass of new charged scalars H^\pm . In Appendix A we show how this result, together with Eqs. (16) and (18), can be used to write μ and λ_{1-7} as functions of the physical parameters we have just presented.

Defining $\tilde{H} = (h, H_1, H_2)$, the couplings involving three CP-even scalars can be generically written as

$$\mathcal{L}_{3\tilde{H}} = -v \frac{\lambda_{ijk}}{S_{ijk}} \tilde{H}_i \tilde{H}_j \tilde{H}_k, \tag{22}$$

where the coefficients λ_{ijk} are symmetric under index interchange. The symmetry factors S_{ijk} are equal to 1 if

all indices are different, 2 if two indices are equal, or 6 if $i = j = k$. The three-scalar interactions involving the pseudoscalar A^0 and the charged scalars H^\pm are

$$\mathcal{L}_{\tilde{H}A^0A^0} = -\frac{v}{2} \sum_{i=1}^3 g_{\tilde{H}_i A^0 A^0} \tilde{H}_i A^0 A^0, \quad (23)$$

$$\mathcal{L}_{\tilde{H}H^+H^-} = -v \sum_{i=1}^3 g_{\tilde{H}_i H^+ H^-} \tilde{H}_i H^+ H^-, \quad (24)$$

respectively. The coefficients λ_{ijk} , $g_{\tilde{H}_i A^0 A^0}$ and $g_{\tilde{H}_i H^+ H^-}$ are collected in Appendix B.

The gauge-boson masses and the gauge-scalar interactions can be obtained from the scalar kinetic terms

$$\mathcal{L} = |D_\mu \Phi_1|^2 + |D_\mu \Phi_2|^2 + |D_\mu \chi|^2, \quad (25)$$

with the covariant derivatives defined as

$$\begin{aligned} D_\mu \Phi_1 &= \left(\partial_\mu - igW_\mu^a \frac{\tau^a}{2} - \frac{1}{2} ig' B_\mu - ig_{Z'} Y'_{\Phi_1} B'_\mu \right) \Phi_1, \\ D_\mu \Phi_2 &= \left(\partial_\mu - igW_\mu^a \frac{\tau^a}{2} - \frac{1}{2} ig' B_\mu \right) \Phi_2, \\ D_\mu \chi &= (\partial_\mu - ig_{Z'} Y'_\chi B'_\mu) \chi. \end{aligned} \quad (26)$$

As usual, W_μ^a and B_μ are the SM gauge fields, while B'_μ is the one corresponding to the new $U(1)'$ symmetry. Notice that $Y'_{\Phi_1} = Y'_\chi = 9Y'_q$, as discussed above. As in the SM, the W -boson mass is

$$m_W^2 = \frac{g^2}{4} v^2, \quad (27)$$

whereas for the neutral gauge bosons we have, in the (W_μ^3, B_μ, B'_μ) basis, the mass matrix

$$\begin{pmatrix} \frac{g^2}{4} v^2 & -\frac{gg'}{4} v^2 & -\frac{gg_{Z'}}{2} Y'_\chi v^2 c_\beta^2 \\ -\frac{gg'}{4} v^2 & \frac{g'^2}{4} v^2 & \frac{g'g_{Z'}}{2} Y'_\chi v^2 c_\beta^2 \\ -\frac{gg_{Z'}}{2} Y'_\chi v^2 c_\beta^2 & \frac{g'g_{Z'}}{2} Y'_\chi v^2 c_\beta^2 & g_{Z'}^2 Y_\chi'^2 (u^2 + v^2 c_\beta^2) \end{pmatrix}. \quad (28)$$

Similarly to the SM, one can write

$$\begin{pmatrix} W_\mu^3 \\ B_\mu \end{pmatrix} = \begin{pmatrix} s_W & c_W \\ c_W & -s_W \end{pmatrix} \begin{pmatrix} A_\mu \\ Z_\mu^0 \end{pmatrix} \quad (29)$$

with $c_W = \cos \theta_W$, $s_W = \sin \theta_W$, θ_W being the weak mixing angle. The A_μ field is massless and corresponds to the physical photon. For the two remaining fields the mass matrix is

$$\begin{pmatrix} m_{ZZ}^2 & m_{ZZ'}^2 \\ m_{Z'Z}^2 & m_{Z'Z'}^2 \end{pmatrix}, \quad (30)$$

where

$$\begin{aligned} m_{ZZ}^2 &= \frac{1}{4} g_1^2 v^2 = \frac{m_W^2}{c_W^2}, \\ m_{ZZ'}^2 &= -\frac{1}{2} g_1 g_{Z'} Y'_\chi v^2 c_\beta^2, \\ m_{Z'Z'}^2 &= (g_{Z'} Y'_\chi)^2 (u^2 + v^2 c_\beta^2), \end{aligned} \quad (31)$$

with $g_1 = g/c_W$. The diagonalisation of this matrix is

$$\begin{pmatrix} Z_\mu^0 \\ B'_\mu \end{pmatrix} = \begin{pmatrix} c_Z & -s_Z \\ s_Z & c_Z \end{pmatrix} \begin{pmatrix} Z_\mu \\ Z'_\mu \end{pmatrix}, \quad (32)$$

with $s_Z = \sin \theta_Z$, $c_Z = \cos \theta_Z$, θ_Z being the $Z-Z'$ mixing angle. The masses of the SM Z boson and the new Z' correspond to the two non-zero eigenvalues,

$$\begin{aligned} m_{Z,Z'}^2 &= \frac{1}{2} \left[m_{ZZ}^2 + m_{Z'Z'}^2 \pm (m_{ZZ}^2 - m_{Z'Z'}^2) \right. \\ &\quad \left. \times ((m_{Z'Z'}^2 - m_{ZZ}^2)^2 + 4m_{ZZ'}^4)^{1/2} \right]. \end{aligned} \quad (33)$$

In the limit of small $Z-Z'$ mixing, i.e. $\theta_Z \ll 1$, the masses of Z and Z' can be approximated as:

$$\begin{aligned} m_Z^2 &\simeq \frac{m_W^2}{c_W^2} \left(1 - \frac{v^2 c_\beta^4}{u^2 + v^2 c_\beta^2} \right), \\ m_{Z'}^2 &\simeq (g_{Z'} Y'_\chi)^2 (u^2 + v^2 c_\beta^2), \end{aligned} \quad (34)$$

while for θ_Z one has

$$\tan \theta_Z \simeq \frac{g_{Z'} Y'_\chi m_W v c_\beta^2}{m_{Z'}^2 c_W}. \quad (35)$$

The interaction of the Z boson with fermions receives a small correction due to $Z-Z'$ mixing,

$$\mathcal{L} = g_1 \bar{\psi} [g_1 (T_3 - s_W^2 Q) c_Z + g_{Z'} Y' s_Z] \gamma^\mu \psi Z_\mu, \quad (36)$$

with T_3 the third isospin component, Q the electric charge and Y' the $U(1)'$ hypercharge of the field ψ . The interaction of the Z' boson with quarks is

$$\mathcal{L} = g_{Z'} \bar{q} \gamma^\mu (y_L P_L + y_R P_R) q Z'_\mu, \quad (37)$$

where the left- and right-handed couplings are

$$\begin{aligned} y_L &= Y'_q c_Z - \frac{g_1}{g_{Z'}} (T_3 - Q s_W^2) s_Z, \\ y_R &= Y'_q c_Z + \frac{g_1}{g_{Z'}} Q s_W^2 s_Z. \end{aligned} \quad (38)$$

The lagrangian terms involving two gauge bosons and one scalar can be written as

$$\begin{aligned} \mathcal{L} &= g_{W^+W^- \tilde{H}_i} W^{-\mu} W_\mu^+ \tilde{H}_i + g_{ZZ \tilde{H}_i} Z^\mu Z_\mu \tilde{H}_i \\ &\quad + g_{ZZ' \tilde{H}_i} Z^\mu Z'_\mu \tilde{H}_i + (g_{ZW^\pm H^\pm} Z^\mu W_\mu^\pm H^\mp \\ &\quad + g_{Z'W^\pm H^\pm} Z'^\mu W_\mu^\pm H^\mp + \text{h.c.}) \end{aligned} \quad (39)$$

with

$$\begin{aligned}
g_{W^+W^-\tilde{H}_i} &= \frac{g^2 v}{2} (O_{1i} c_\beta + O_{2i} s_\beta), \\
g_{ZZ\tilde{H}_i} &= \frac{g_1^2 v}{4} (O_{1i} c_\beta + O_{2i} s_\beta) c_Z^2 \\
&\quad - g_1 g_{Z'} Y'_\chi v O_{1i} c_\beta c_Z s_Z \\
&\quad + g_{Z'}^2 Y_\chi'^2 (O_{1i} v c_\beta + O_{3i} u) s_Z^2, \\
g_{ZZ'\tilde{H}_i} &= -\frac{g_1^2 v}{2} (O_{1i} c_\beta + O_{2i} s_\beta) c_Z s_Z \\
&\quad - g_1 g_{Z'} Y'_\chi v O_{1i} c_\beta (c_Z^2 - s_Z^2) \\
&\quad + 2g_{Z'}^2 Y_\chi'^2 (O_{1i} v c_\beta + O_{3i} u) c_Z s_Z, \\
g_{Z'W^\pm H^\pm} &= -g g_{Z'} Y'_\chi v c_\beta s_\beta s_Z, \\
g_{Z'W^\pm H^\pm} &= -g g_{Z'} Y'_\chi v c_\beta s_\beta c_Z. \tag{40}
\end{aligned}$$

The Lagrangian terms with two scalars and one gauge boson are

$$\begin{aligned}
\mathcal{L} &= g_{Z\tilde{H}_i A^0} \tilde{H}_i \overleftrightarrow{\partial}_\mu A^0 Z^\mu + g_{Z'\tilde{H}_i A^0} \tilde{H}_i \overleftrightarrow{\partial}_\mu A^0 Z'^\mu \\
&\quad + g_{\gamma H^+ H^-} A^\mu H^+ \overleftrightarrow{\partial}_\mu H^- + g_{ZH^+ H^-} Z^\mu H^+ \overleftrightarrow{\partial}_\mu H^- \\
&\quad + g_{Z'H^+ H^-} Z'^\mu H^+ \overleftrightarrow{\partial}_\mu H^- + (g_{W^\pm \tilde{H}_i H^\pm} W^{+\mu} H^- \overleftrightarrow{\partial}_\mu \tilde{H}_i \\
&\quad + g_{W^\pm A^0 H^\pm} W^{+\mu} H^- \overleftrightarrow{\partial}_\mu A^0 + \text{h.c.}), \tag{41}
\end{aligned}$$

with

$$\begin{aligned}
g_{Z\tilde{H}_i A^0} &= \frac{g_1}{2} (O_{1i} s_\beta - O_{2i} c_\beta) s_\alpha c_Z \\
&\quad - g_{Z'} Y'_\chi (O_{1i} s_\beta s_\alpha + O_{3i} c_\alpha) s_Z, \\
g_{Z'\tilde{H}_i A^0} &= \frac{g_1}{2} (O_{2i} c_\beta - O_{1i} s_\beta) s_\alpha s_Z \\
&\quad - g_{Z'} Y'_\chi (O_{1i} s_\beta s_\alpha + O_{3i} c_\alpha) c_Z, \\
g_{\gamma H^+ H^-} &= i e, \\
g_{ZH^+ H^-} &= i \left[g_1 \left(\frac{1}{2} - s_W^2 \right) c_Z + g_{Z'} Y'_\chi s_\beta^2 c_Z \right], \\
g_{Z'H^+ H^-} &= i \left[-g_1 \left(\frac{1}{2} - s_W^2 \right) s_Z + g_{Z'} Y'_\chi s_\beta^2 c_Z \right], \\
g_{W^\pm \tilde{H}_i H^\pm} &= i \frac{g}{2} (-O_{1i} s_\beta + O_{2i} c_\beta), \\
g_{W^\pm A^0 H^\pm} &= \frac{g}{2} s_\alpha. \tag{42}
\end{aligned}$$

The above interactions allow to compute the different partial decay widths for the Z' boson and the scalars. These are collected in Appendix C.

III. PARAMETER SPACE SCAN

We use the code `ScannerS` [23] to scan the parameter space of the UN2HDM and to check whether the points in parameter space are allowed or excluded at the 95% confidence level (CL). In this analysis, the following constraints are taken into account:

- Theoretical constraints imposed by perturbative unitarity, boundedness from below and vacuum stability conditions [15]. These are applied after calculating the parameters of the scalar potential using the equations collected in Appendix A;
- Electroweak precision constraints, which use fit results for the oblique parameters S , T and U shown in [24]. These are compared with UN2HDM predictions for those parameters, implemented in `ScannerS` using the results of [25, 26];
- Flavour constraints based on fit results of [24], which set limits in the $(m_{H^\pm}, \tan \beta)$ plane;
- Compatibility of the SM-like scalar with the properties of the experimentally discovered Higgs boson;
- Bounds from direct searches for beyond SM scalars.

To incorporate the constraints mentioned in the last two points, `ScannerS` provides an interface to `HiggsSignals` [27, 28] and `HiggsBounds` [29–33]. Some of the inputs required by those two tools are the branching ratios of all scalars. These are computed by the library `N2HDECAY` [34], which is also included in `ScannerS`¹.

Parameter	Range
m_h	125.09 GeV
$m_{H_1}, m_{H_2}, m_{A^0}, m_{H^\pm}$	see Section IV
$\tan \beta$	[0, 20]
$c(hVV)^2$	[0.9, 1.0]
$c(ht\bar{t})^2$	[0.8, 1.2]
$\text{sign}(O_{31})$	{-1, 1}
O_{32}	[-1, 1]
2HDM type	I
$m_{Z'}$	2 TeV
$g_{Z'} Y'_q$	0.1

TABLE II. List of common input parameters for the parameter space scan.

In order to increase the efficiency of the scan [23], we parameterise the mixing matrix of CP-even scalars using (i) the effective couplings of the SM-like Higgs boson h to top quarks, $c(ht\bar{t})$; (ii) the effective coupling to SM gauge bosons $c(hVV)$, with $V = W, Z$; O_{32} and $\text{sign}(O_{31})$. Using these four parameters we are able to compute the three mixing angles in O , c.f. (17) while

¹ Due to the differences between the scalar potential of the UN2HDM and the one in [34], the triple scalar couplings in Appendix B have to be implemented in `ScannerS`. In contrast, no changes are done to the couplings between scalars and SM gauge bosons, since they are equal to those found in Eqs. (40) and (42) in the limit $\theta_Z \ll 1$.

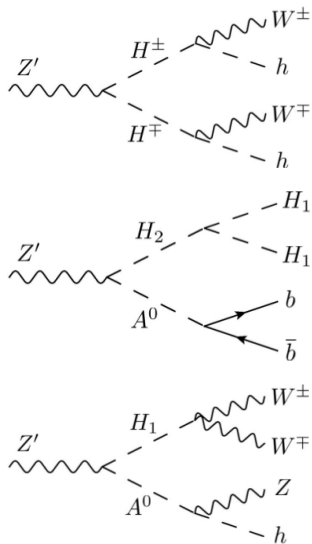


FIG. 1. Feynman diagrams for the Z' cascade decays studied in each benchmark scenario.

simultaneously constraining the couplings of h to be SM-like. The type of 2HDM used is also an input, specifying the flavour constraints applied. Finally, the parameters $m_{Z'}$ and $g_{Z'}Y'_q$ are required to extract the VEV of the singlet and the $Z - Z'$ mixing angle. We set a reference mass $M_{Z'} = 2$ TeV. The Z' production cross section is determined by the product $g_{Z'}Y'_q$, which we set to 0.1. The list of common parameters used for all chosen benchmarks is presented in Table II, together with their varying ranges. (The ranges for the new scalar masses are different for the various benchmarks examined, as shown in the next section.) With the parameter values shown in Table II, we get $u \sim 2.2$ TeV and $\theta_Z < 10^{-3}$.

For the parameter-space points allowed by the aforementioned constraints, we compute the Z' cross section into SM final states, especially for $Z' \rightarrow W^+W^-$, $Z' \rightarrow Zh$ and $Z' \rightarrow t\bar{t}$, to require agreement with direct searches. Searches of Z' decaying into dijets are also considered but they are less constraining [35].

IV. BENCHMARKS

Multiboson signals are generated in the UN2HDM by cascade decay of the Z' boson into new scalars, which subsequently decay into W , Z bosons or other scalars. We focus on three scenarios that are representative of various types of multiboson signals:

1. $Z' \rightarrow H^+H^-$, with $H^\pm \rightarrow W^\pm h$;
2. $Z' \rightarrow H_2A^0$, with $H_2 \rightarrow H_1H_1$ and $A^0 \rightarrow b\bar{b}$;
3. $Z' \rightarrow H_1A^0$, $H_1 \rightarrow W^+W^-$ and $A^0 \rightarrow Zh$;

The Feynman diagrams for these decays are shown in Fig. 1. In scenario 1, for m_{H^\pm} of few hundreds of GeV,

	Benchmark 1	Benchmark 2	Benchmark 3
m_{H_1}	[30,1000]	[20,40]	[150,250]
m_{H_2}	[30,1000]	[90,110]	[250,1000]
m_{A^0}	[30,1000]	[90,110]	[200,300]
m_{H^\pm}	[500,700]	[80,1000]	[80,1000]

TABLE III. Mass ranges (in GeV) of the new scalars used in each benchmark.

the four bosons in the final state are resolved, yielding a quadriboson signal not experimentally covered. In scenario 2, with H_2 and A_0 relatively light, the decay $H_2 \rightarrow H_1H_1 \rightarrow 4b$ produces a four-pronged jet, while $A_0 \rightarrow b\bar{b}$ produces a two-pronged jet. Finally, scenario 3 with relatively-light H_1 and A^0 produces two four-pronged jets (when $h^0 \rightarrow b\bar{b}$) with different mass and flavour content. The latter two are partly covered by a search for a heavy resonance decaying into two massive jets [39] that unfortunately does not consider jet substructure for the discrimination against SM dijet background. Table IV collects the range for scalar masses used for the scan in each benchmark scenario. The scalar branching ratios are computed by N2HDECAY, while for the branching ratios of the Z' boson we use the partial widths collected in Appendix C. In all cases, we consider the new leptons to be heavy enough not to play any role in Z' decays.

A. Scenario 1

In this case, the branching ratio for $Z' \rightarrow H^+H^-$ can be up to 0.3, while fulfilling the direct limits on other Z' decay modes (and possible improvements with more data). Fig. 2 (top) shows the branching ratio for $Z' \rightarrow H^+H^-$ versus $Z' \rightarrow Zh$. The vertical line corresponds to the experimental upper limit at 95% CL derived for this mass from current searches [36], assuming $g_{Z'}Y'_q = 0.1$. A similar plot can be obtained for $Z' \rightarrow H^+H^-$ versus $Z' \rightarrow W^+W^-$, but the allowed area has similar shape and the limit [37] is less constraining. It is remarkable that $Z' \rightarrow H^+H^-$ can be sizeable while $Z' \rightarrow W^+W^-$ and $Z' \rightarrow Zh$ vanish. The reason is that the interactions mediating the latter two modes are proportional to powers of the VEV v_1 of the scalar doublet that has non-vanishing hypercharge, either explicitly from $\cos\beta$ factors, or through the $Z - Z'$ mixing. The limits from $Z' \rightarrow t\bar{t}$ [38] do not constrain the parameter space allowed by **ScannerS** (bottom panel), but an improvement by more than a factor of two would exclude the value of $g_{Z'}Y'_q$ used in this benchmark.

Requiring agreement with direct searches, the branching ratios for $Z' \rightarrow H^+H^-$ versus $H^\pm \rightarrow W^\pm h$ are presented in Fig. 3. One can see that the H^\pm can mostly decay into $W^\pm h$ while having $\text{BR}(Z' \rightarrow H^+H^-) \simeq 0.3$. As a result, the maximum branching ratio for $Z' \rightarrow$

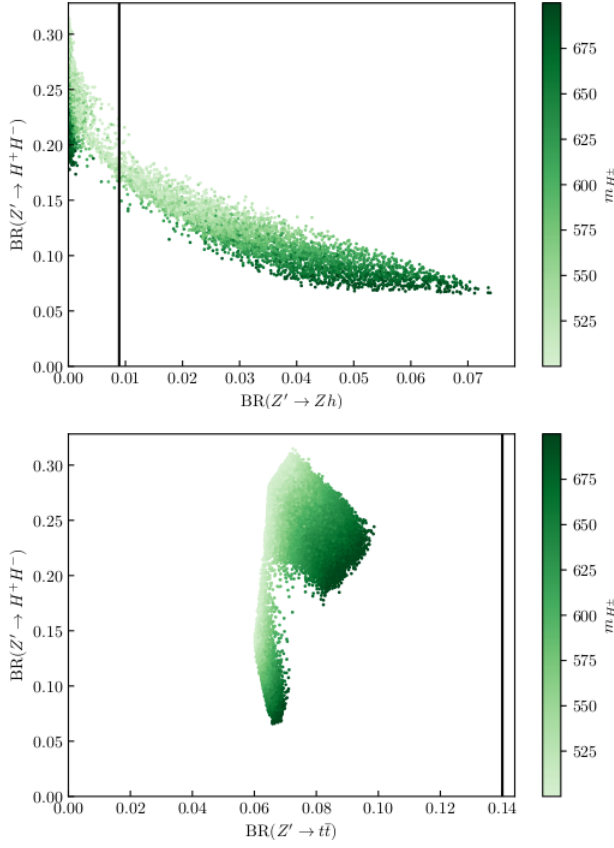


FIG. 2. Branching ratio for $Z' \rightarrow H^+H^-$ versus $Z' \rightarrow Zh$ (top) and $Z' \rightarrow t\bar{t}$ (bottom) resulting from the parameter space scan. The vertical lines correspond to the experimental upper bounds. The colour grading is related to the m_{H^\pm} value as shown on the right.

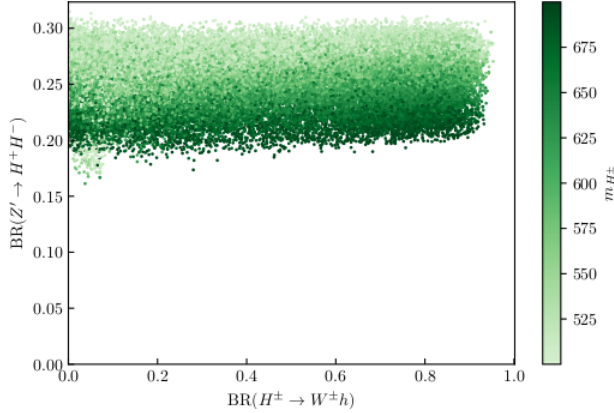


FIG. 3. Branching ratios for $Z' \rightarrow H^+H^-$ versus $H^\pm \rightarrow W^\pm h$ resulting from the parameter space scan. The colour grading is related to the m_{H^\pm} value as shown on the right.

W^+hW^-h reached is 0.27, leading to a cross section times branching ratio of 29 fb for $g_{Z'}Y'_q = 0.1$.

B. Scenario 2

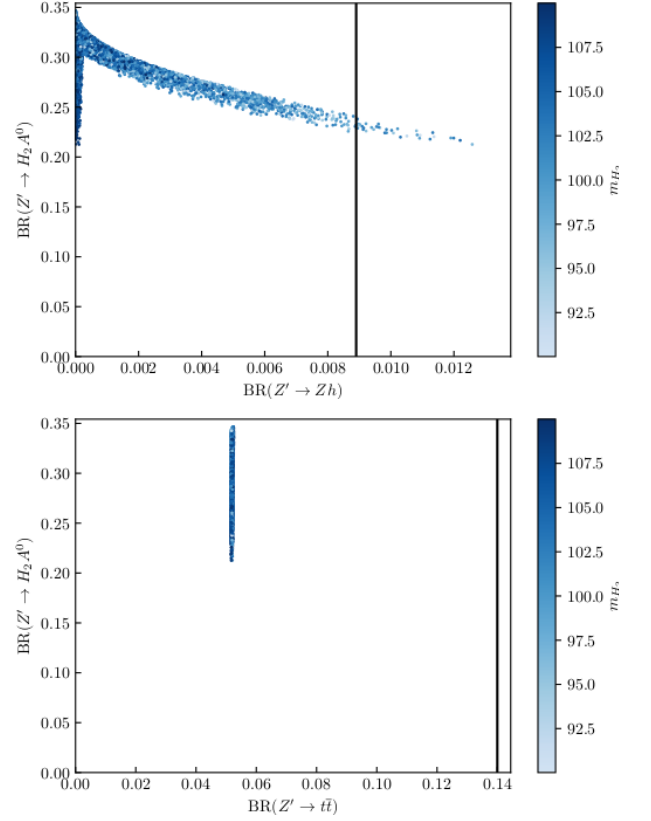


FIG. 4. Branching ratio for $Z' \rightarrow H_2A^0$ versus $Z' \rightarrow Zh$ (top) and $Z' \rightarrow t\bar{t}$ (bottom) resulting from the parameter space scan. The vertical lines correspond to the experimental upper bound. The colour grading is related to the m_{H_2} value as shown on the right.

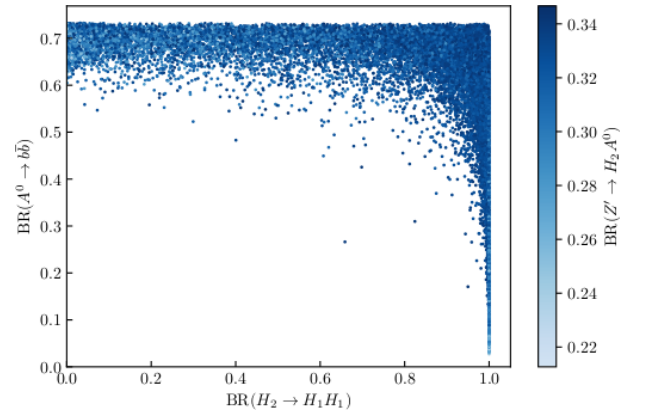


FIG. 5. Branching ratios for $A^0 \rightarrow b\bar{b}$ versus $H_2 \rightarrow H_1H_1$ resulting from the parameter space scan. The colour grading is related to the value of $\text{BR}(Z' \rightarrow H_2A^0)$ as shown on the right.

In this scenario, the branching ratio for $Z' \rightarrow H_2 A^0$ can range up to 0.35, while fulfilling the direct limits on other Z' decay modes (and possible improvements with more data). Fig. 4 shows the branching ratio for $Z' \rightarrow H_2 A^0$ versus $Z' \rightarrow Zh$. The analogous figure considering $Z' \rightarrow W^+ W^-$ has similar shape, but the current limit does not further constrain the parameter space, and is omitted for brevity. Once more, we observe that the decay into SM bosons $Z' \rightarrow W^+ W^-$, $Z' \rightarrow Zh$ can have negligible rates while $Z' \rightarrow H_2 A^0$ is sizeable. This is again because the latter decay is not suppressed when the VEV v_1 is small. Direct limits from $Z' \rightarrow t\bar{t}$ do not constrain further the parameter space allowed by **ScannerS**, as seen in the bottom panel. However, an improvement by more than a factor of two would make this constraint relevant. The results have little dependence on the masses of H_2 and A^0 , which range within a narrow interval [90, 110] GeV in this scenario.

The size of the signal in this scenario is determined — besides the Z' cross section production that is fixed by its mass and $g_{Z'} Y'_q$ — by the three different branching ratios for $Z' \rightarrow H_2 A^0$, $H_2 \rightarrow H_1 H_1$ and $A^0 \rightarrow b\bar{b}$. (Since H_1 is the lightest scalar, it decays to $b\bar{b}$ nearly all the time.) We present in Fig. 5 the branching ratios for $A^0 \rightarrow b\bar{b}$ versus $H_2 \rightarrow H_1 H_1$, with the colour corresponding to $\text{Br}(Z' \rightarrow H_2 A^0)$, for points fulfilling the limit from $Z' \rightarrow Zh$. Clearly, all three branching ratios can be sizeable, with a maximum combined branching ratio for $Z' \rightarrow H_1 H_1 b\bar{b}$ of 0.25, leading to a product of the cross section times branching ratio of 27 fb for $g_{Z'} Y'_q = 0.1$.

C. Scenario 3

The Z' decay mode considered in this scenario is similar to the previous one, but considering instead the lightest new scalar H_1 , and larger masses for H_1 and A^0 to allow for other decay modes. The branching ratio for $Z' \rightarrow H_1 A^0$ can also range up to 0.35, see Fig. 6 (top). The only direct limit that partially constrains the parameter space allowed by **ScannerS** is $Z' \rightarrow Zh$. As discussed in the previous two benchmarks, future improvements of the limit on $Z' \rightarrow t\bar{t}$ would become constraining (bottom panel).

The size of the multiboson signal in this scenario is determined by the three different branching ratios for $Z' \rightarrow H_1 A^0$, $H_1 \rightarrow W^+ W^-$ and $A^0 \rightarrow Zh$. We present in Fig. 7 the branching ratios for $A^0 \rightarrow Zh$ versus $H_1 \rightarrow W^+ W^-$, with the colour grading corresponding to the value of $\text{Br}(Z' \rightarrow H_1 A^0)$, for points fulfilling the direct limit from $Z' \rightarrow Zh$. We point out that the high density of points around $\text{Br}(H_1 \rightarrow W^+ W^-) \simeq 0.7$ is motivated by the fact that, when both channels are kinematically open, $\text{Br}(H_1 \rightarrow W^+ W^-) \simeq 2 \times \text{Br}(H_1 \rightarrow ZZ)$. The latter is suppressed for H_1 masses below the ZZ threshold, thus the rate into $W^+ W^-$ can range up to unity for the H_1 masses considered. Overall, the three branching ratios can be sizeable, with a maximum combined branching ratio for $Z' \rightarrow W^+ W^- Zh$ of 0.29, leading to a cross section times branching ratio of 31 fb for $g_{Z'} Y'_q = 0.1$.

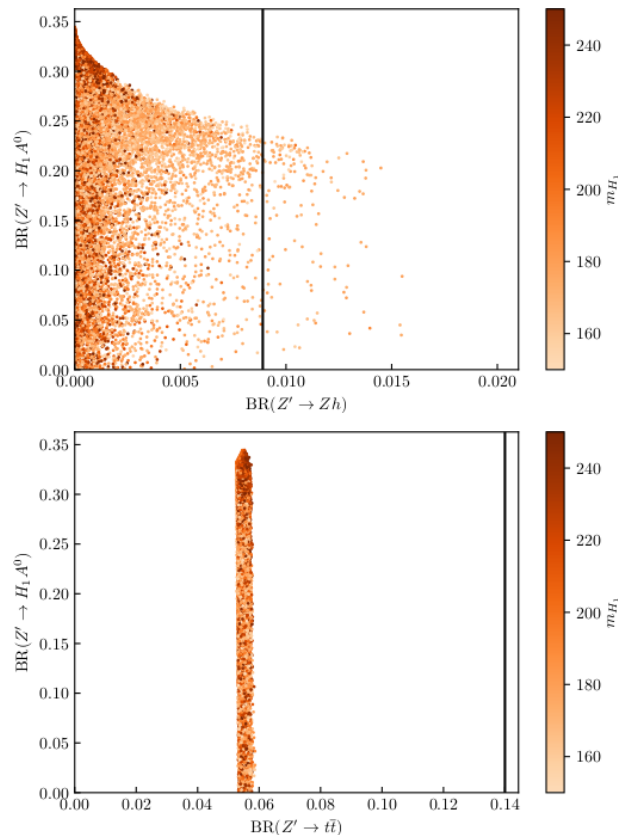


FIG. 6. Branching ratio for $Z' \rightarrow H_1 A^0$ versus $Z' \rightarrow Zh$ (top) and $Z' \rightarrow t\bar{t}$ (bottom) resulting from the parameter space scan. The vertical lines correspond to the experimental upper bound. The colour grading is related to the m_{H_2} value as shown on the right.

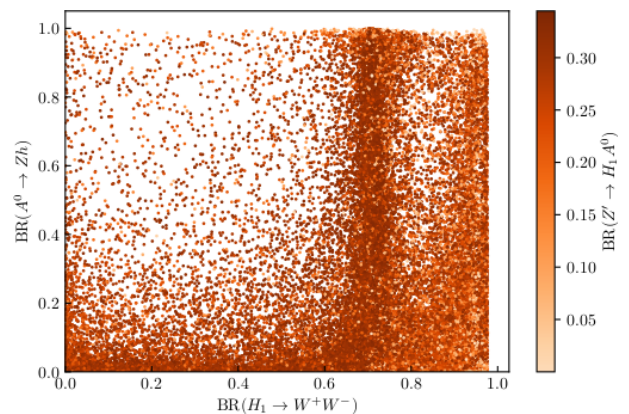


FIG. 7. Branching ratios for $A^0 \rightarrow Zh$ versus $H_1 \rightarrow WW$ resulting from the parameter space scan. The colour grading is related to the value of $\text{Br}(Z' \rightarrow H_1 A^0)$ as shown on the right.

V. DISCUSSION

The LHC has set very stringent limits on the production of new resonances decaying into SM particles, with around 140 fb^{-1} of Run 2 data collected at 13 TeV. Still, many final states remain to be explored. Conspicuously, these unexplored signals might be sizeable, yet compatible with existing limits. We have explored three scenarios for the production of multiboson signals from the decay of a Z' boson. With cross sections times branching ratio around 30 fb in the three scenarios, around 4000 multiboson events could be produced with the collected luminosity.

A wide variety of signal topologies is possible, depending on the decay modes of the W , Z and h bosons in the final state. Given the high performance achieved by jet taggers [40, 41], already the hadronic decays of SM bosons (which have the largest branching ratios) are expected to provide a good sensitivity to these types of signals. We note that semileptonic signals are also possible, for example from $H_1 \rightarrow W^+W^-$, when one of the W bosons decays hadronically and the other one leptonically. A detailed study is out of the scope of this work.

In order to be sensitive to the multiboson signals proposed in this work, dedicated analyses or anomaly-detection methods are required. The signal produced in scenario 2 has a dijet topology, with one jet having four-pronged structure and the other one two-pronged. In scenario 3, when at least one of the W bosons and the Z/h decay hadronically, the signal also has a dijet topology. It has been demonstrated that anomaly detection tools such as CWoLa [42, 43] and SOFIE [44] have the potential to uncover such signals. The signal of scenario 1 has four resolved bosons in the final state. This makes its discrimination from the background technically more demanding, as it features a 4-body resonance plus two intermediate two-body resonances. It is likely that the SOFIE or CATHODE [45] methods are efficient in its detection too.

In summary, the results in this paper show that there are complex new physics signals that could be at reach with already collected LHC data, which motivates the use of generic tools and anomaly-detection strategies to pursue the discovery of any type of physics beyond the SM. We stress that such signals appear naturally in the context of popular SM extensions for which studies are usually focused only on the most simple final-state topologies (mostly direct decays into SM particles).

ACKNOWLEDGEMENTS

We thank Rui Santos and Duarte Azevedo for communications on some aspects related to the `ScannerS` code. The work of J.A.A.S. has been supported by MICINN project PID2019-110058GB-C21 and CEX2020-001007-S funded by MCIN/AEI/10.13039/501100011033 and by ERDF. F.R.J. and J.F.S. acknowledge Fundação para

a Ciência e a Tecnologia (FCT, Portugal) for financial support through the projects UIDB/00777/2020, UIDP/00777/2020, CERN/FIS-PAR/0004/2019, and PTDC/FIS-PAR/29436/2017. The work of J.F.S. is supported by the FCT grant SFRH/BD/143891/2019.

Appendix A: Higgs potential parameters

As we have noted in Section II, the scalar potential of the UN2HDM has eleven parameters, which correspond to the same number of physical parameters of the scalar sector of the theory. The VEV of the scalar singlet can be expressed as a function of other physical parameters of the UN2HDM. From (33) it follows that

$$m_Z^2 + m_{Z'}^2 = m_{ZZ}^2 + m_{Z'Z'}^2. \quad (\text{A1})$$

Using the explicit expressions of these matrix elements in Eq. (31), we obtain

$$u^2 = \frac{m_Z^2 + m_{Z'}^2 - m_W^2/c_W^2}{(g_Z Y')^2} - v^2 c_\beta^2. \quad (\text{A2})$$

By inverting Eq. (16), we can write μ as a function of VEV parameters and the pseudoscalar mass m_{A^0} :

$$\mu = -\frac{\sqrt{2} u c_\beta s_\beta}{u^2 + v^2 c_\beta^2 s_\beta^2} m_{A^0}^2. \quad (\text{A3})$$

The charged-scalar mass in Eq. (21) can be used to determine λ_4 ,

$$\lambda_4 = -\frac{1}{v^2} \left[m_{H^\pm}^2 + \frac{\sqrt{2} u \mu}{s_\beta c_\beta} \right]. \quad (\text{A4})$$

The remaining λ_i coefficients can be expressed in terms of those parameters using Eq. (18). Defining $\tilde{M} = (m_h^2, m_{H_1}^2, m_{H_2}^2)$,

$$\begin{aligned} \lambda_1 &= \frac{1}{v^2 c_\beta^2} \left[\sum_{i=1}^3 \tilde{M}_i O_{1i}^2 + \frac{u\mu}{\sqrt{2}} \frac{s_\beta}{c_\beta} \right], \\ \lambda_2 &= \frac{1}{v^2 s_\beta^2} \left[\sum_{i=1}^3 \tilde{M}_i O_{2i}^2 + \frac{u\mu}{\sqrt{2}} \frac{c_\beta}{s_\beta} \right], \\ \lambda_3 &= \frac{1}{v^2 c_\beta s_\beta} \left[\sum_{i=1}^3 \tilde{M}_i O_{1i} O_{2i} - \frac{u\mu}{\sqrt{2}} \right] - \lambda_4, \\ \lambda_5 &= \frac{1}{u^2} \left[\sum_{i=1}^3 \tilde{M}_i O_{3i}^2 + \frac{v^2 \mu}{\sqrt{2} u} c_\beta s_\beta \right], \\ \lambda_6 &= \frac{2}{u v c_\beta} \left[\sum_{i=1}^3 \tilde{M}_i O_{1i} O_{3i} - \frac{v\mu}{\sqrt{2}} s_\beta \right], \\ \lambda_7 &= \frac{2}{u v s_\beta} \left[\sum_{i=1}^3 \tilde{M}_i O_{2i} O_{3i} - \frac{v\mu}{\sqrt{2}} c_\beta \right]. \end{aligned} \quad (\text{A5})$$

Appendix B: Triple scalar couplings

In the weak basis $w = (\rho_1, \rho_2, \rho_3, \eta_1, \eta_2, \eta_3)$, the lagrangian terms involving three scalar fields can be written as

$$\mathcal{L}_{3H} = - \sum_{p \leq q \leq r}^6 v C_{pqr}^n w_p w_q w_r. \quad (\text{B1})$$

The nonzero coefficients C_{pqr}^n are given by

$$\begin{aligned} C_{111}^n &= C_{144}^n = \frac{1}{2} \lambda_1 c_\beta, \\ C_{112}^n &= C_{244}^n = \frac{1}{2} (\lambda_3 + \lambda_4) s_\beta, \\ C_{113}^n &= C_{344}^n = \frac{1}{4} \lambda_6 \frac{u}{v}, \\ C_{122}^n &= C_{155}^n = \frac{1}{2} (\lambda_3 + \lambda_4) c_\beta, \\ C_{123}^n &= C_{246}^n = C_{345}^n = \frac{1}{v\sqrt{2}} \mu, \\ C_{133}^n &= C_{166}^n = \frac{1}{4} \lambda_6 c_\beta, \\ C_{156} &= -\frac{1}{v\sqrt{2}} \mu, \\ C_{222}^n &= C_{255}^n = \frac{1}{2} \lambda_2 s_\beta, \\ C_{223}^n &= C_{355}^n = \frac{1}{4} \lambda_7 \frac{u}{v}, \\ C_{233}^n &= C_{266}^n = \frac{1}{4} \lambda_7 s_\beta, \\ C_{333}^n &= C_{366}^n = \frac{1}{2} \lambda_5 \frac{u}{v}. \end{aligned} \quad (\text{B2})$$

The interactions with three scalar fields are thus either of the form

$$\mathcal{L}_{3\tilde{H}} = - \sum_{p \leq q \leq r} v C_{pqr}^n \rho_p \rho_q \rho_r, \quad (\text{B3})$$

with three CP-even fields, or

$$\mathcal{L}_{\tilde{H}A^0A^0} = - \sum_{p \leq q \leq r} v C_{pqr}^n \rho_p \eta_{q-3} \eta_{r-3}. \quad (\text{B4})$$

with one CP-even and two CP-odd fields. The weak eigenstates can be written in terms of mass eigenstates as $\rho_i = O_{ia} \tilde{H}_a$ and $\eta_i = R_{i3} A^0$, respectively. Therefore,

$$\mathcal{L}_{3\tilde{H}} = - \sum v C_{pqr}^n O_{pa} O_{qb} O_{rc} \tilde{H}_a \tilde{H}_b \tilde{H}_c \quad (\text{B5})$$

where the sums over a, b, c and $p \leq q \leq r$ run from 1 to 3, and

$$\mathcal{L}_{\tilde{H}A^0A^0} = - \sum v C_{pqr}^n O_{pa} R_{q-3,3} R_{r-3,3} \tilde{H}_a A^0 A^0, \quad (\text{B6})$$

with a and p running from 1 to 3 and $q \leq r$ from 4 to 6. We write

$$\lambda_{ijk} = \sum_{p \leq q \leq r, (s)} C_{pqr}^n O_{ps_1} O_{qs_2} O_{rs_3}, \quad (\text{B7})$$

where $(s) \equiv (s_1, s_2, s_3)$ represents the set of all permutations of the indices i, j and k . Introducing a symmetry factor S_{ijk} to account for multiple counting of the same terms, we arrive at the expression in (22). The couplings between a CP-even neutral scalar and two CP-odd ones are given by

$$g_{\tilde{H}_i A^0 A^0} = \sum_{p=1}^3 \sum_{4 \leq q \leq r}^6 v C_{pqr}^n O_{pi} R_{q-3,3} R_{r-3,3}. \quad (\text{B8})$$

The interactions of one neutral scalar and two charged ones are, in the weak basis,

$$\mathcal{L}_{\tilde{H}H^+H^-} = - \sum_{p=1}^6 \sum_{q,r=1}^2 v C_{pqr}^c w_p \phi_q^+ \phi_r^-. \quad (\text{B9})$$

The nonzero coefficients C_{pqr}^c are

$$\begin{aligned} C_{111}^c &= \lambda_1 c_\beta, \\ C_{112}^c &= C_{121}^c = \frac{1}{2} \lambda_4 s_\beta, \\ C_{122}^c &= \lambda_3 c_\beta, \\ C_{211}^c &= \lambda_3 s_\beta, \\ C_{212}^c &= C_{221}^c = \frac{1}{2} \lambda_4 c_\beta, \\ C_{222}^c &= \lambda_2 s_\beta, \\ C_{311}^c &= \frac{1}{2} \lambda_6 \frac{u}{v}, \\ C_{312}^c &= C_{321}^c = \frac{1}{\sqrt{2}v} \mu, \\ C_{322}^c &= \frac{1}{2} \lambda_7 \frac{u}{v}, \\ C_{412}^c &= -C_{421}^c = -\frac{i}{2} \lambda_4 s_\beta, \\ C_{512}^c &= -C_{521}^c = \frac{i}{2} \lambda_4 c_\beta, \\ C_{612}^c &= -C_{621}^c = -\frac{i}{\sqrt{2}v} \mu. \end{aligned} \quad (\text{B10})$$

Using $\phi_i^\pm = U_{i2} H^\pm$, with U in Eq. (20), in the mass-eigenstate basis the terms of Eq. (B9) that could lead to a coupling between A^0, H^+ and H^- cancel. On the other hand, the Lagrangian involving one CP-even field and two charged ones can be written as

$$\mathcal{L}_{\tilde{H}H^+H^-} = - \sum v C_{pqr}^c O_{pa} U_{q2} U_{r2} \tilde{H}_a H^+ H^-. \quad (\text{B11})$$

The index p in Eq. (B11) runs from 1 to 3 whereas q and r are either 1 or 2. The couplings of CP-even neutral scalars to charged scalars are given by

$$g_{\tilde{H}_i H^+ H^-} = \sum_{p=1}^3 \sum_{q,r=1}^2 v C_{pqr}^c O_{pi} U_{q2} U_{r2}. \quad (\text{B12})$$

Appendix C: Partial widths

In this appendix we collect for completeness the partial widths for the relevant decay of the new particles introduced in the UN2HDM. The partial widths of the Z' boson are

$$\begin{aligned}
\Gamma(Z' \rightarrow W^+W^-) &= \frac{g^2 c_W^2 s_z^2 m_{Z'}^5}{192\pi m_W^4} \left(1 - 4 \frac{m_W^2}{m_{Z'}^2}\right)^{3/2} \\
&\times \left(1 + 20 \frac{m_W^2}{m_{Z'}^2} + 12 \frac{m_W^4}{m_{Z'}^4}\right), \\
\Gamma(Z' \rightarrow Z\tilde{H}_i) &= \frac{g_{Z Z' \tilde{H}_i}^2 \lambda^{1/2}(m_{Z'}, m_Z^2, m_{\tilde{H}_i}^2)}{192\pi m_Z^2 m_{Z'}} \\
&\times \left[1 + 10 \frac{m_Z^2}{m_{Z'}^2} - 2 \frac{m_{\tilde{H}_i}^2}{m_{Z'}^2} + \frac{m_Z^4}{m_{Z'}^4} + \frac{m_{\tilde{H}_i}^4}{m_{Z'}^4} - 2 \frac{m_Z^2 m_{\tilde{H}_i}^2}{m_{Z'}^4}\right], \\
\Gamma(Z' \rightarrow W^+H^-) &= \frac{g_{Z' W^\pm H^\pm}^2 \lambda^{1/2}(m_{Z'}, m_W^2, m_{H^\pm}^2)}{192\pi m_Z^2 m_{Z'}} \\
&\left[1 + 10 \frac{m_W^2}{m_{Z'}^2} - 2 \frac{m_{H^\pm}^2}{m_{Z'}^2} + \frac{m_W^4}{m_{Z'}^4} + \frac{m_{H^\pm}^4}{m_{Z'}^4} - 2 \frac{m_W^2 m_{H^\pm}^2}{m_{Z'}^4}\right], \\
\Gamma(Z' \rightarrow \tilde{H}_i A^0) &= \frac{g_{Z' \tilde{H}_i A^0}^2}{48\pi m_{\tilde{H}_i}^5} \lambda^{3/2}(m_{Z'}, m_{\tilde{H}_i}^2, m_{A^0}^2), \\
\Gamma(Z' \rightarrow H^+H^-) &= \frac{g_{Z' H^+ H^-}^2}{48\pi m_{Z'}^5} \lambda^{3/2}(m_{Z'}, m_{H^\pm}^2, m_{H^\pm}^2), \\
\Gamma(Z' \rightarrow q\bar{q}) &= \frac{N_c g_{Z' q}^2 m_{Z'}}{24\pi} \left(1 - 4 \frac{m_q^2}{m_{Z'}^2}\right)^{1/2} \\
&\times \left[(y_L^2 + y_R^2) \left(1 - \frac{m_q^2}{m_{Z'}^2}\right) + 6y_L y_R \frac{m_q^2}{m_{Z'}^2} \right], \quad (C1)
\end{aligned}$$

with the usual kinematical function

$$\lambda(x, y, z) = x^2 + y^2 + z^2 - 2xy - 2xz - 2yz. \quad (C2)$$

The partial widths of the scalars are

$$\begin{aligned}
\Gamma(\tilde{H}_i \rightarrow f\bar{f}) &= \frac{N_c}{8\pi} \frac{m_f^2}{v^2 \sin^2 \beta} m_{\tilde{H}_i} O_{2i}^2 \left[1 - 4 \frac{m_f^2}{m_{\tilde{H}_i}^2}\right]^{3/2}, \\
\Gamma(\tilde{H}_i \rightarrow W^+W^-) &= \frac{g_{WW\tilde{H}_i}^2 m_{\tilde{H}_i}^3}{64\pi m_W^4} \left[1 - 4 \frac{m_W^2}{m_{\tilde{H}_i}^2}\right]^{1/2} \\
&\times \left[1 - 4 \frac{m_W^2}{m_{\tilde{H}_i}^2} + 12 \frac{m_W^4}{m_{\tilde{H}_i}^4}\right], \\
\Gamma(\tilde{H}_i \rightarrow ZZ) &= \frac{g_{ZZ\tilde{H}_i}^2 m_{\tilde{H}_i}^3}{32\pi m_Z^4} \left[1 - 4 \frac{m_Z^2}{m_{\tilde{H}_i}^2}\right]^{1/2} \\
&\times \left[1 - 4 \frac{m_Z^2}{m_{\tilde{H}_i}^2} + 12 \frac{m_Z^4}{m_{\tilde{H}_i}^4}\right], \\
\Gamma(\tilde{H}_i \rightarrow A^0 Z) &= \frac{g_{Z\tilde{H}_i A^0}^2}{16\pi m_{\tilde{H}_i}^3 m_Z^2} \lambda^{3/2}(m_{\tilde{H}_i}^2, m_Z^2, m_{A^0}^2), \\
\Gamma(\tilde{H}_i \rightarrow W^+H^-) &= \frac{g_{W^\pm \tilde{H}_i H^\pm}^2}{16\pi m_{\tilde{H}_i}^3 m_W^2} \lambda^{3/2}(m_{\tilde{H}_i}^2, m_W^2, m_{H^\pm}^2). \quad (C3)
\end{aligned}$$

-
- [1] J. A. Aguilar-Saavedra, JHEP **10** (2015), 099 [arXiv:1506.06739 [hep-ph]].
- [2] J. A. Aguilar-Saavedra and F. R. Joaquim, JHEP **01**, 183 (2016) [arXiv:1512.00396 [hep-ph]].
- [3] G. Aad et al. [ATLAS Collaboration], JHEP **12**, 055 (2015) [arXiv:1506.00962 [hep-ex]].
- [4] A. Tumasyan et al. [CMS Collaboration], To be submitted to Phys. Rev. Lett. [arXiv:2201.08476 [hep-ex]].
- [5] K. Agashe et al., JHEP **11**, 027 (2018) [arXiv:1809.07334 [hep-ph]].
- [6] K. Agashe et al., Phys. Rev. D **99**, no.7, 075016 (2019) [arXiv:1711.09920 [hep-ph]].
- [7] J. A. Aguilar-Saavedra, JHEP **05** (2017), 066 [arXiv:1703.06153 [hep-ph]].
- [8] ATLAS Collaboration, ATLAS-CONF-2016-055.
- [9] M. Aaboud et al. [CMS Collaboration], Phys. Rev. D **97**, no.7, 072006 (2018) [arXiv:1708.05379 [hep-ex]].
- [10] J. A. Aguilar-Saavedra, Eur. Phys. J. C **77**, no.10, 703 (2017) [arXiv:1705.07885 [hep-ph]].
- [11] J. A. Aguilar-Saavedra and F. R. Joaquim, JHEP **10**, 237 (2019) [arXiv:1905.12651 [hep-ph]].
- [12] J. A. Aguilar-Saavedra and F. R. Joaquim, Eur. Phys. J. C **80**, no.5, 403 (2020) [arXiv:2002.07697 [hep-ph]].
- [13] CMS Collaboration, CMS-PAS-B2G-20-009.
- [14] C. Y. Chen, M. Freid, M. Sher, Phys. Rev. D **89**, no.7, 075009 (2014) [arXiv:1312.3949 [hep-ph]].
- [15] M. Mühlleitner, M. O. P. Sampaio, R. Santos and J. Wittbrodt, JHEP **03**, 094 (2017) [arXiv:1612.01309 [hep-ph]].
- [16] V. Keus, N. Koivunen and K. Tuominen, JHEP **09**, 059 (2018) [arXiv:1712.09613 [hep-ph]].
- [17] S. von Buddenbrock et al., J. Phys. G **46**, no.11, 115001 (2019) [arXiv:1809.06344 [hep-ph]].
- [18] P. M. Ferreira, M. Mühlleitner, R. Santos, G. Weiglein and J. Wittbrodt, JHEP **09**, 006 (2019) [arXiv:1905.10234 [hep-ph]].
- [19] T. Biekötter, M. Chakraborti and S. Heinemeyer, Eur. Phys. J. C **80**, no.1, 2 (2020) [arXiv:1903.11661 [hep-ph]].

- [20] I. Engeln, P. M. Ferreira, M. Mühlleitner, R. Santos, and J. Wittbrodt, *JHEP* **08**, 085 (2020) [arXiv:2004.05382 [hep-ph]].
- [21] P. Langacker, *Rev. Mod. Phys.* **81**, 1199 (2009) [arXiv:0801.1345 [hep-ph]].
- [22] S. Caron, J. A. Casas, J. Quilis and R. Ruiz de Austri, *JHEP* **12** (2018), 126 [arXiv:1807.07921 [hep-ph]].
- [23] M. Mühlleitner, M. O. P. Sampaio, R. Santos and J. Wittbrodt, *Eur. Phys. J. C* **82**, no.3, 198 (2022) [arXiv:2007.02985 [hep-ph]].
- [24] J. Haller et al., *Eur. Phys. J. C* **78**, no.8, 675 (2018) [arXiv:1803.01853 [hep-ph]].
- [25] W. Grimus, L. Lavoura, O. M. Ogreid and P. Osland, *J. Phys. G* **35**, 075001 (2008) [arXiv:0711.4022 [hep-ph]].
- [26] W. Grimus, L. Lavoura, O. M. Ogreid and P. Osland, *Nucl. Phys. B* **801**, 81 (2008) [arXiv:0802.4353 [hep-ph]].
- [27] P. Bechtle, S. Heinemeyer, O. Stål, T. Stefaniak and G. Weiglein, *Eur. Phys. J. C* **74**, no.2, 2711 (2014) [arXiv:1305.1933 [hep-ph]].
- [28] P. Bechtle et al., *Eur. Phys. J. C* **81**, no.2, 145 (2021) [arXiv:2012.09197 [hep-ph]].
- [29] P. Bechtle, O. Brein, S. Heinemeyer, G. Weiglein and K. E. Williams, *Comput. Phys. Commun.* **181**, 138 (2010) [arXiv:0811.4169 [hep-ph]].
- [30] P. Bechtle, O. Brein, S. Heinemeyer, G. Weiglein and K. E. Williams, *Comput. Phys. Commun.* **182**, 2605 (2011) [arXiv:1102.1898 [hep-ph]].
- [31] P. Bechtle et al., *Eur. Phys. J. C* **74**, no.3, 2693 (2014) [arXiv:1311.0055 [hep-ph]].
- [32] P. Bechtle, S. Heinemeyer, O. Stål, T. Stefaniak and G. Weiglein *Eur. Phys. J. C* **75**, no.9, 421 (2015) [arXiv:1507.06706 [hep-ph]].
- [33] P. Bechtle et al., *Eur. Phys. J. C* **80**, no.12, 1211 (2020) [arXiv:2006.06007 [hep-ph]].
- [34] I. Engeln, M. Mühlleitner and J. Wittbrodt, *Comput. Phys. Commun.* **234**, 256 (2019) [arXiv:1805.00966 [hep-ph]].
- [35] J. A. Aguilar-Saavedra, I. Lara, D. E. Lopez-Fogliani and C. Muñoz, *Eur. Phys. J. C* **81**, no.5, 443 (2021) [arXiv:2101.05565 [hep-ph]].
- [36] A. M. Sirunyan *et al.* [CMS Collaboration], *Eur. Phys. J. C* **81** (2021) no.8, 688 [arXiv:2102.08198 [hep-ex]].
- [37] G. Aad *et al.* [ATLAS Collaboration], *JHEP* **09** (2019), 091 [erratum: *JHEP* **06** (2020), 042] [arXiv:1906.08589 [hep-ex]].
- [38] G. Aad *et al.* [ATLAS Collaboration], *JHEP* **10** (2020), 061 [arXiv:2005.05138 [hep-ex]].
- [39] G. Aad *et al.* [ATLAS Collaboration], *Phys. Rev. Lett.* **125** (2020) no.13, 131801 [arXiv:2005.02983 [hep-ex]].
- [40] J. A. Aguilar-Saavedra, F. R. Joaquim and J. F. Seabra, *JHEP* **03** (2021), 012 [arXiv:2008.12792 [hep-ph]].
- [41] O. Atkinson, A. Bhardwaj, C. Englert, V. S. Ngairangbam and M. Spannowsky, *JHEP* **08** (2021), 080 [arXiv:2105.07988 [hep-ph]].
- [42] J. H. Collins, K. Howe and B. Nachman, *Phys. Rev. Lett.* **121** (2018) no.24, 241803 [arXiv:1805.02664 [hep-ph]].
- [43] J. H. Collins, K. Howe and B. Nachman, *Phys. Rev. D* **99** (2019) no.1, 014038 [arXiv:1902.02634 [hep-ph]].
- [44] J. A. Aguilar-Saavedra, *Eur. Phys. J. C* **82** (2022) no.2, 130 [arXiv:2111.02647 [hep-ph]].
- [45] A. Hallin, J. Isaacson, G. Kasieczka, C. Krause, B. Nachman, T. Quadfasel, M. Schlaffer, D. Shih and M. Sommerhalder, [arXiv:2109.00546 [hep-ph]].